AIAA JOURNAL
Vol. 40, No. 6, June 2002

Heterogeneous Propellant Combustion

T. L. Jackson* and J. Buckmaster†
University of Illinois at Urbana–Champaign, Urbana, Illinois 61801

In earlier work it has been shown that spheres of various sizes can be randomly packed to simulate the morphology of ammonium perchlorate (AP)/binder heterogeneous propellants. A model is now formulated in which propellants defined in this way can be burnt, allowing for complete coupling between the gas-phase physics, the condensed-phase physics, and the unsteady nonuniform regression of the propellant surface. The gas-phase kinetics is represented by a two-step model with parameters fitted to experimental data for the one-dimensional combustion of pure AP and the one-dimensional combustion of a fine-AP/binder blend. In the discussion of the pure AP fits, the issue of intrinsic instabilities arises, and these are explored using nonlinear direct numerical simulation and a numerical linear-stability strategy. Results for two-dimensional heterogeneous burning show that surface regions where the AP and binder can mix regress more rapidly than those dominated by AP; local extinction can occur where the binder dominates. Time variations in the integrated flux-based equivalence ratio are shown to be large. Variations in the average burning rate with pressure are consistent with the (three-dimensional) experimental record.

Nomenclature

c_p	=	specific heat
$D_{1,2}$	=	reaction rate constants
d_j	=	diameter of the jth particle class
E	=	activation energy
f	=	surface function
M	=	mass flux
N_j	=	number in the jth particle class
$n_{1,2}$	=	pressure exponents in the reaction rates
Pr	=	Prandtl number
P_0	=	constant background pressure
p	=	spatially varying flow pressure
$Q_{g1,g2}$	=	heats of reaction
Q_s	=	heat of decomposition
R_u	=	universal gas constant
$R_{1,2}$	=	gas-phase reaction rates
r_b	=	surface regression rate
T	=	temperature
T_*	=	flame temperature
t	=	time
u, v, w	=	velocity components
X	=	mass fraction of ammonium perchlorate (AP) in the gas phase
Y	=	mass fraction of binder
Z	=	mass fraction of AP decomposition products
α	=	mass fraction of AP in the condensed phase
α_v	=	volume fraction of AP in the condensed phase
β	=	mass-based stoichiometric coefficient
η	=	surface function
λ	=	heat conductivity
ρ	=	density

Subscripts

AP	=	ammonium perchlorate
B	=	binder
c	=	condensed phase
g	=	gas phase
s	=	surface

Received 28 March 2001; revision received 2 November 2001; accepted for publication 14 December 2001.

*Senior Research Scientist, Center for the Simulation of Advanced Rockets, 1304 West Springfield Avenue; tlj@csar.uiuc.edu.

†Professor, Department of Aeronautical and Astronautical Engineering, 104 South Wright Street; limey@uiuc.edu. Associate Fellow AIAA.

I. Introduction

WE are concerned with the numerical calculation of the combustion field supported by heterogeneous propellants that consist of ammonium perchlorate (AP) particles embedded in a fuel binder. Although a great deal of important work has been done on this problem, a significant obstacle has been the lack of a model of the propellant morphology. Recently, however, a random packing algorithm has been used to pack spheres of various sizes in cubes, periodically arranged, and it has been suggested that these structures can be used for that purpose.[1,2] Whereas it is true that AP particles are not spherical, the algorithm can be used to generate packs for which the size distribution (the number fraction of particles in any diameter range) and the packing fraction (the volume fraction of the cube occupied by the AP) are the same as those for industrial propellant packs.

An example is shown in Fig. 1. This is a Miller pack[3] (SD-III-88-24) consisting of 31.58% (by weight) of a 200-μm AP cut, 42.11% of a 50-μm AP cut, and 13.68% of a 20-μm AP cut. Each cut contains a wide range of particle sizes, and in constructing Fig. 1 we have used data supplied by the Thiokol Corp. (courtesy of R. Bennett) (see Ref. 2). The packing fraction achieved by the algorithm is 0.7698, which differs insignificantly from the true value of 0.766.

A slice through the cube of Fig. 1, or similar cubes, defines boundary data for the propellant combustion field. A slice through a 100,000 particle pack is shown in Fig. 2. Here the size distribution is defined by a single cut, the 200-μm AP Thiokol Corp. data, and the packing fraction is 0.6537. This is much smaller than the stoichiometric value achieved by the pack of Fig. 1, because the 200-μm AP data do not include a significant number of small particles.

The cube of Fig. 2 has sides of length 7.46 mm, and a line through the cube parallel to any face intersects $\sim(100{,}000)^{1/3} \approx 46$ particles. Thus, even for such a small cube, a large number of mesh points are required to resolve the condensed-phase thermal field and the gas-phase combustion field. The resolution demands are even higher when a pack of wide-ranging sizes is used, as in the Miller pack,[3] of Fig. 1. Undoubtedly, homogenization strategies will be needed to deal with the smallest particles, but we shall avoid the issue in this paper by examining small domains in a two-dimensional context, random disk packs in squares, periodically arrayed. The Thiokol Corp. 200-μm AP data (Table 1) can then be used to generate packs with packing fractions of 79%, and six examples are shown in Fig. 3. (That a disk pack leads to higher packing fractions than a pack of spheres is to be expected when

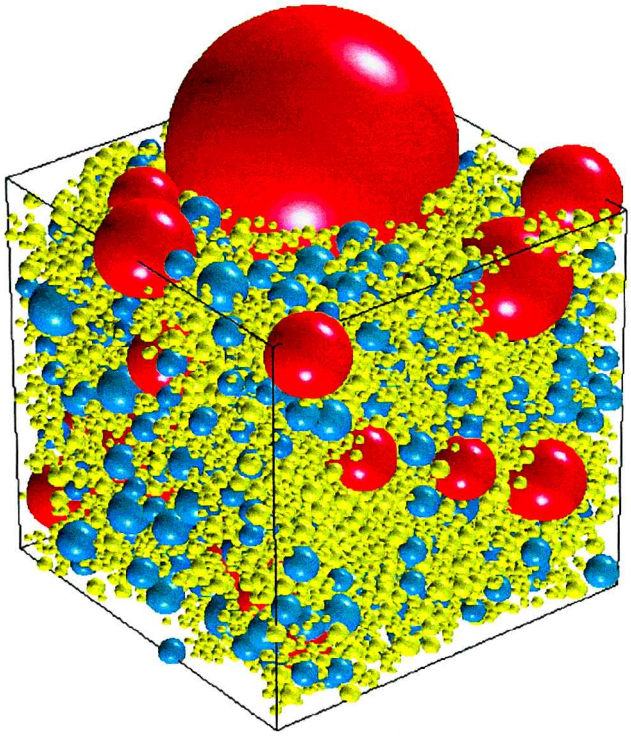

Fig. 1 Miller pack[3] SD-III-88-24 (10,000 particles) (courtesy of S. Kochevets): gold spheres have diameters in the range 5–15 μm; blue, 16–42 μm; and red, 46–211 μm. Partial pack with packing fraction 0.595 is shown for clarity.

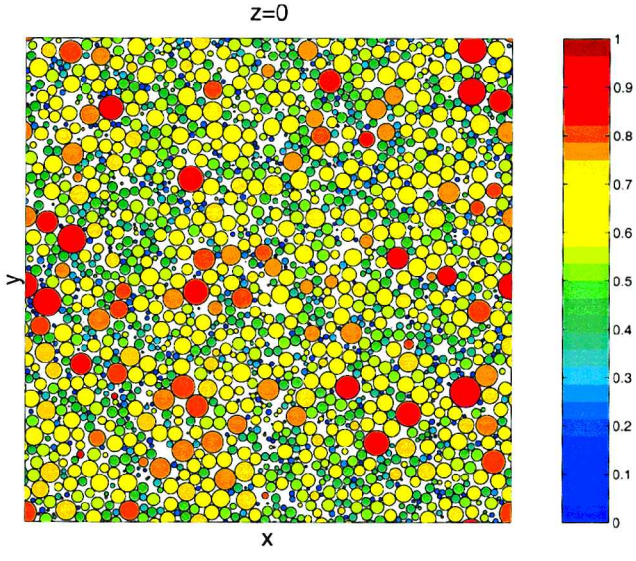

Fig. 2 Central slice through a 100,000 particle pack (courtesy of S. Kochevets), packing fraction 0.6537. This uses the 28 different diameters of the Thiokol Corp. 200-μm AP data, with a random selection strategy[2]; each diameter is assigned a different color.

one notes that the inscribed circle occupies a fraction $\pi/4$ of a square, whereas the inscribed sphere occupies a fraction $\pi/6$ of a cube.) By scaling the particle diameters, we can generate pack squares of any desired size, and we have chosen a scaling (see column 2 of Table 1) so that the side of each square is 1 mm. These are the foundations on which our combustion calculations are built.

II. Fully Coupled Problem of Propellant Burning

An early and justifiably famous discussion of heterogeneous propellant combustion can be found in Ref. 4 (the Beckstead–Derr–Price model). This accounts for many of the important features of

Table 1 For 101 particles, 200-μm packing data (number of particles, diameter)[a]

d_j	Scaled d_j[b]	N_j
337.400	220.744	1
309.400	202.425	1
283.700	185.611	2
260.650	170.530	3
239.050	156.398	4
218.750	143.117	5
200.600	131.243	5
183.950	120.349	6
168.700	110.372	6
154.700	101.212	6
141.850	92.805	6
130.100	85.118	6
119.300	78.052	5
109.400	71.575	5
100.330	65.641	5
91.980	60.178	5
84.350	55.186	5
77.350	50.606	5
70.930	46.406	5
65.045	42.556	5
59.645	39.023	5
54.695	35.784	5

[a]Only 22 different diameters used (cf. Fig. 2) because consolidation of large particles is necessary for such a small pack.[2]
[b]Scaled diameters generate two-dimensional packs of side 1 mm; packs used in the combustion calculations.

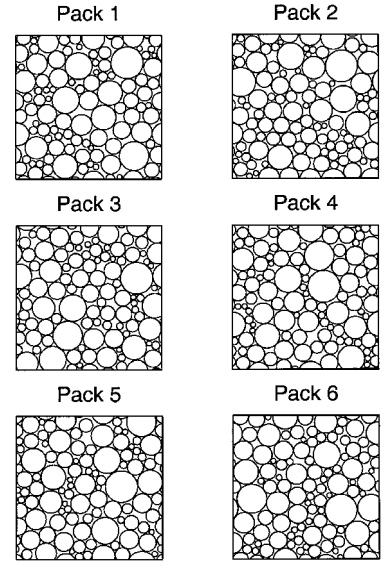

Fig. 3 Number of random disk packs generated using the Thiokol Corp. 200-μm AP data (Table 1).

the combustion field but, being essentially one dimensional, has significant deficiencies. More recent attempts incorporate multidimensional calculations of the gas phase,[5] but only Ref. 6 accounts properly for coupling between the condensed phase and the gas phase across a nonplanar unsteadily moving interface (the propellant surface). However, the study of Ref. 6 examines, not random propellant packs, but periodic sandwiches, alternating slices of fuel binder and AP. It is possible that sandwich calculations will be of value for model validation at some future time, but only when experimental data become available that approximates that for periodic sandwiches. The single sandwich studies of Price et al.[7] and Price,[8] for example, are subject to lateral fluxes of heat and mass, fluxes of unknown magnitude. In the present paper, we apply the fully coupled strategy to the burning of a random pack. Although in the final analysis we shall describe only two-dimensional calculations, our formulation will be three dimensional because it is the foundation for three-dimensional calculations that we plan to report later.

Condensed Phase

In the condensed phase we solve the heat equation

$$c_p \rho_c \frac{\partial T}{\partial t} = \nabla \cdot (\lambda_c \nabla T) \tag{1}$$

where we have assumed, for simplicity, that the specific heat is the same as that for the gas; the values of ρ_c and λ_c are assigned according to whether a point is located in the binder or in an AP particle. The morphology is described by a level-set function $\psi(x, y)$, defined by the packing algorithm, which is nonnegative in the AP and negative in the binder. Thus,

$$\rho_c = \begin{cases} \rho_{\mathrm{AP}} \\ \rho_B \end{cases}, \qquad \lambda_c = \begin{cases} \lambda_{\mathrm{AP}}, & \psi \geq 0 \\ \lambda_B, & \psi < 0 \end{cases} \tag{2}$$

Propagation of the Surface

The surface regresses normal to itself with a speed r_b (>0), where we assume that r_b is defined by simple pyrolysis laws, namely,

$$r_b = \begin{cases} r_{\mathrm{AP}} = A_{\mathrm{AP}} \exp\{-E_{\mathrm{AP}}/R_u T_{\mathrm{AP},s}\}, & \psi \geq 0 \\ r_B = A_B \exp\{-E_B/R_u T_{B,s}\}, & \psi < 0 \end{cases} \tag{3}$$

where $T_{,s}$ is the surface temperature. The activation energies are large, so that modest variations of $T_{,s}$ lead to large changes in the regression rate. It is for this reason that propellant surface temperatures have typical values, narrowly defined.

It is convenient to represent the surface by

$$\eta(x, y, z, t) = 0 \tag{4}$$

where η is governed by the kinematic relation

$$\frac{\partial \eta}{\partial t} + \boldsymbol{v} \cdot \nabla \eta = 0, \qquad \boldsymbol{v} = -r_b \boldsymbol{n}, \qquad n = \frac{\nabla \eta}{|\nabla \eta|} \tag{5}$$

where $\boldsymbol{n}$ is a unit vector, normal to the surface, pointing into the gas. We assume, further, that η can be written in the form

$$\eta \equiv y - f(x, z, t) \tag{6}$$

where f, the surface location, is a single-valued function of (x, z). Thus, y is nominally measured perpendicular to the propellant surface, and x and z are nominally measured parallel to the surface. Should f not be single valued, should a portion of the surface overhang another portion, the computational difficulties are significantly increased, and we do not examine that situation at this time. Now Eq. (5a) can be written

$$f_t + r_b \sqrt{1 + f_x^2 + f_z^2} = 0 \tag{7}$$

which is a simple Hamilton–Jacobi equation.

Gas Phase

Gas-phase processes are described by the zero-Mach-number Navier–Stokes equations for a variable density gas, the energy equation, species equations, and suitable chemical kinetics.

We use the simplest possible kinetic scheme, represented by

$$\mathrm{AP}(X) \xrightarrow{R_1} \text{decomposition products}(Z)$$

$$\beta Z + \text{binder}(Y) \xrightarrow{R_2} \text{final products} \tag{8}$$

where

$$R_1 = D_1 P_0^{n_1} X \exp\{-E_1/R_u T\} \tag{9a}$$

$$R_2 = D_2 P_0^{n_2} Z Y \exp\{-E_2/R_u T\} \tag{9b}$$

Because rates (9) do not correspond to real reactions but are representative of many, the usual relations between the stoichiometric coefficients, the pressure exponents, and the exponents of the reacting species do not have to be satisfied. In due course, we hope to implement more sophisticated kinetic schemes, guided perhaps by the kind of data emerging from the program reported in Ref. 9.

The corresponding equations for X, Y, Z, and T are

$$\mathcal{L}(X, Y, Z) = (-R_1, -R_2, R_1 - \beta R_2) \tag{10}$$

$$\mathcal{L}(T) = \left(Q_{g1} R_1 + Q_{g2} R_2 + \frac{\mathrm{d}P_0}{\mathrm{d}t} \right) \Big/ c_p \tag{11}$$

where

$$\mathcal{L} \equiv \rho \frac{\mathrm{D}}{\mathrm{D}t} - \nabla \cdot \left(\frac{\lambda_g}{c_p} \nabla \right) \tag{12}$$

We have assumed that all Lewis numbers are equal to 1, but temperature-dependent transport is accounted for,[10] namely,

$$\lambda_g = 1.08 \times 10^{-4} T + 0.0133 \text{ W/mK} \tag{13}$$

when T is assigned in degrees Kelvin. Here c_p is assumed to be constant.

The parameter β in Eqs. (8) and (10) is the overall mass-based AP/binder stoichiometric ratio: β kg of AP, X, are required for the stoichiometric consumption of 1 kg of binder, Y. The packing fraction of each of the packs shown in Fig. 3 is 79%, and β is chosen so that these packs are stoichiometric. Because AP has a specific gravity of 1.95 and the binder a specific gravity of 0.92, it follows that $\beta = 7.97$.

Later we shall describe how the kinetic parameters of Eqs. (9) are determined.

The remaining equations are

$$P_0(t) = \frac{\rho R_u T}{\mathrm{MW}} \tag{14}$$

$$\frac{\partial \rho}{\partial t} + \nabla \cdot (\rho \boldsymbol{q}) = 0, \qquad \boldsymbol{q} = (u, v, w) = (q_1, q_2, q_3) \tag{15}$$

$$\rho \frac{\mathrm{D}q_i}{\mathrm{D}t} = -\frac{\partial p}{\partial x_i} + \frac{\partial}{\partial x_j} \left(\frac{Pr \lambda_g}{c_p} \frac{\partial q_i}{\partial x_j} \right) + \frac{\partial}{\partial x_j} \left(\frac{Pr \lambda_g}{c_p} \frac{\partial q_j}{\partial x_i} \right) - \frac{2}{3} \frac{\partial}{\partial x_i} \left(\frac{Pr \lambda_g}{c_p} \frac{\partial q_k}{\partial x_k} \right) \tag{16}$$

where the Prandtl number is assumed to be constant and the molecular weight is MW.

Conditions at Propellant Surface

The propellant surface is an interface between the condensed phase and the gas phase, and certain conditions are imposed there that relate the solution in one phase to that in the other. These include continuity of tangential velocity so that

$$[\boldsymbol{q} \times \boldsymbol{n}] = 0 \tag{17}$$

which, because $\boldsymbol{q} = 0$ in the condensed phase, can be written

$$u + v f_x = 0, \qquad w + v f_z = 0, \qquad -u f_z + w f_x = 0 \tag{18}$$

Also the normal mass flux is continuous so that

$$[M] = [\rho(q_n + r_b)] = 0 \tag{19}$$

and this can be written as

$$M = \rho_c r_b = -\frac{\rho_c f_t}{\sqrt{1 + f_x^2 + f_z^2}} = \frac{\rho_g \bar{v}}{\sqrt{1 + f_x^2 + f_z^2}} \tag{20}$$

where

$$\bar{v} = v - u f_x - w f_z - f_t \tag{21}$$

Continuing, energy conservation at the surface has the form

$$[\lambda \boldsymbol{n} \cdot \nabla T] = -Q_s M \tag{22}$$

and the species flux condition is

$$M[Y_i] = [(\lambda/c_p)\boldsymbol{n}\cdot\nabla Y_i] \tag{23}$$

In all of these formulas $[\cdot] \equiv (\cdot)_g - (\cdot)_c$; Y_i refers to the species X, Y, or Z; M is the mass flux normal to the surface; $Q_s > 0$ (<0) for an exothermic (endothermic) process; and both r_b and Q_s take on different values according to whether the surface is AP or binder.

Mapping

It is computationally convenient to use the mapping

$$x, y, z, t \to x, \eta = y - f(x, z, t), z, t \tag{24}$$

so that the surface is flat in the new coordinates. Then

$$\frac{\partial}{\partial x} \to \frac{\partial}{\partial x} - f_x\frac{\partial}{\partial \eta}, \qquad \frac{\partial}{\partial y} \to \frac{\partial}{\partial \eta}, \qquad \frac{\partial}{\partial z} \to \frac{\partial}{\partial z} - f_z\frac{\partial}{\partial \eta}$$

$$\frac{\partial}{\partial t} \to \frac{\partial}{\partial t} - f_t\frac{\partial}{\partial \eta}, \qquad \frac{\mathrm{D}}{\mathrm{D}t} \to \frac{\partial}{\partial t} + u\frac{\partial}{\partial x} + \bar{v}\frac{\partial}{\partial \eta} + w\frac{\partial}{\partial z} \tag{25}$$

These are used to transform both the field equations and the surface conditions.

Oseen Approximation

Although our code can include the Navier–Stokes equation (16), an Oseen approximation significantly reduces the computational burden, and calculations for sandwich propellants attest to its accuracy (see Ref. 6). This approximation is defined by

$$u = w = 0, \qquad \rho\bar{v} = -\rho_c f_t \tag{26}$$

which violates the no-slip conditions (18), but is consistent with Eq. (20). Note that the equation of mass conservation (15) becomes

$$\frac{\partial \rho}{\partial t} + \frac{\partial}{\partial \eta}(\rho\bar{v}) = 0 \tag{27}$$

consistent with Eq. (26b) when gas-phase processes are assumed to be quasi steady, which is a familiar characteristic of propellant burning. [Then $\mathrm{d}P_0/\mathrm{d}t$ is neglected in Eq. (11).]

Flame Temperatures

There are two flame-temperatures of significance to our discussion. The adiabatic flame temperature for pure AP decomposition is

$$T_{*\mathrm{AP}} = T_0 + (1/c_p)(Q_{g1} + Q_{s,\mathrm{AP}}) \tag{28}$$

where T_0 is the propellant supply temperature, the temperature far from the surface. When $T_0 = 300$ K, a suitable choice of $T_{*\mathrm{AP}}$ is 1400 K, and we choose $(Q_{g1} + Q_{s,\mathrm{AP}})$ to be consistent with this.

The adiabatic flame temperature for the heterogeneous propellant is

$$T_{*H} = T_0 + (\alpha/c_p)(Q_{g1} + Q_{s,\mathrm{AP}}) + [(1-\alpha)/c_p](Q_{g2} + Q_{s,B}) \tag{29}$$

where α is the mass fraction of AP in the propellant, so that

$$\alpha = \beta/(1+\beta) \tag{30}$$

A suitable choice for T_{*H} constrains the value of $(Q_{g2} + Q_{s,B})$.

Parameter Choices

Table 2 shows the parameter choices that we have made, typical of those that can be found in the literature. Some of them are certain, for example, ρ_{AP} (Ref. 11), and others less so. For example, a wide range of choices have been proposed for how the overall heat generated by the AP decomposition should be distributed between surface values $Q_{s,\mathrm{AP}}$ and gas-phase values Q_{g1}, an issue that plays a role in the discussion of AP instabilities to be found in a later section.

Note that the choices for the regression rate coefficients A_{AP} and A_B mean that the AP regresses at a speed of 0.287 cm/s when the surface temperature is 865.6 K (Ref. 12) and the binder regresses at the same speed when the surface temperature is 915.6 K.

Table 2 Parameter values[4,5,10,12]

Parameter	Value
A_{AP}	$0.287\exp\{E_{\mathrm{AP}}/R_u/865.6\}$ cm/s
A_B	$0.287\exp\{E_B/R_u/915.6\}$ cm/s
c_p	0.3 kcal/kg K
E_{AP}/R_u	11,000 K
E_B/R_u	7,500 K
MW	26
Pr	1
Q_{g1}	430 kcal/kg
Q_{g2}	3,338 kcal/kg
$Q_{s,\mathrm{AP}}$	−100 kcal/kg
$Q_{s,B}$	−47 kcal/kg
R_u	1.9859 kcal/kmol · K
T_0	300 K
$T_{*\mathrm{AP}}$	1,400 K
T_{*H}	2,500 K
α_v	0.79
α	0.8886
β	7.97
λ_{AP}	0.405 W/m · K
λ_B	0.276 W/m · K
ρ_{AP}	1,950 kg/m^3
ρ_B	920 kg /m^3

The gas-phase kinetic data are determined by direct appeal to experiment. When one considers a heterogeneous propellant, there are two special cases for which the combustion field is one dimensional: 1) no binder, so that only the AP decomposition occurs (reaction R_1), and 2) the propellant consists of a blend of fine AP and binder that supports a double-structured deflagration: AP decomposition R_1 followed by a premixed R_2 reaction. Experimental data are available for the first of these,[12] and results partly based on experiment are available for the second,[13] and these data permit the determination of the parameters characterizing R_1 and R_2, Eq. (9).

Thus, consider R_1 and pure AP decomposition. A standard flame-sheet analysis incorporating Eq. (9a) predicts that X is consumed in the sheet at a rate that is proportional to

$$\exp\{-E_1/2R_uT_*\}$$

where T_* is the flame temperature. It follows that the regression rate of the surface has the form

$$c = A\exp\{-E_1/2R_uT_*\} \tag{31}$$

for some constant A, whence

$$\frac{1}{c}\frac{\mathrm{d}c}{\mathrm{d}T_*} = \frac{E_1}{R_uT_*}\cdot\frac{1}{2T_*} \tag{32}$$

Because we assume that the specific heat of the solid differs little from that of the gas (at constant pressure) (obviously more elaborate discussions are possible), a one-degree change in the supply temperature of the solid generates a one-degree change in the flame temperature, and then formula (32) identifies the so-called sensitivity σ. According to Ref. 14, $\sigma = 0.002$ and so, for $T_* = 1400$ K, $E_1/R_u = 8000\ K$, after some minor rounding off.

The flame-sheet analysis implies that the consumption of X depends only on parameters that appear in the diffusion and reaction terms, namely, $D_1P_0^{n1}$, Q_{g1}, E_1, and T_*, and the value of the transport coefficients at the flame sheet. Thus, the regression rate depends only on these parameters and the density of the solid, accurately known. In reality, other parameters play a role, but one that is relatively weak, and so they are not important in the numerical/experimental fit. With the selections from Table 2 and the specification (13) for $\lambda_g(T)$, parameters D_1 and n_1 can then be chosen to match experimental regression rates. Thus, $D_1 = 1.3718\times10^4$ g · cm^{-3}s^{-1}bar^{-n1}, where $n_1 = 1.7$ gives an excellent fit of c vs P in the pressure range 20–70 atm (Fig. 4a). (See Sec. III for a discussion of an issue that arises at higher pressures.)

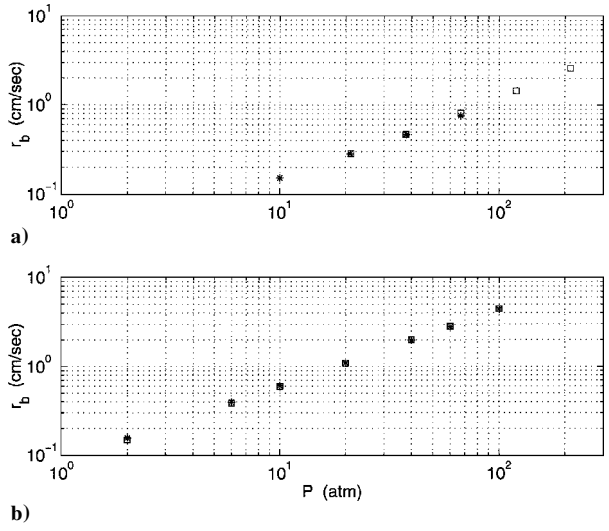

Fig. 4 One-dimensional comparisons with experiment, ∗ numerical: a) □, experimental pure AP data inferred from Ref. 12 and b) □, experimentally based fine AP mix data from Ref. 13, mass fraction of AP = 0.8.

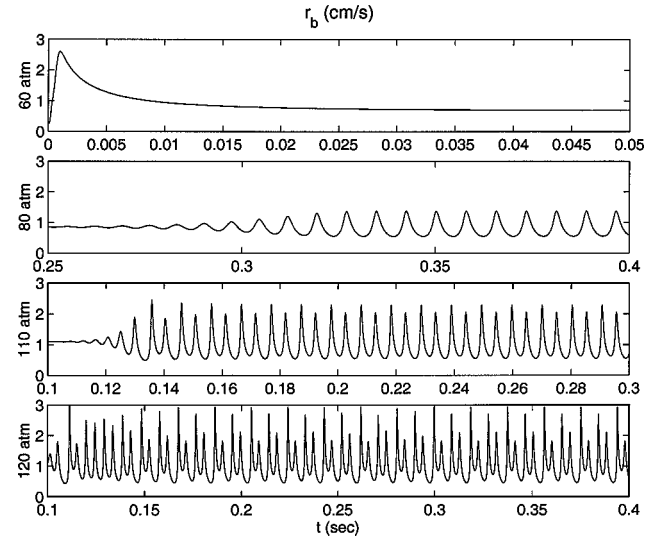

Fig. 5 Variations of the burning rate of pure AP with time, for different pressures.

Our model does not capture the low-pressure self-deflagration limit of AP.

Turning to the stoichiometric AP/binder mix, Z is completely consumed in the second flame sheet, so that here,

$$\sigma = (E_2/R_u T_*) \cdot (1/2T_*) \tag{33}$$

Compare Eq. (32). According to Ref. 13, $\sigma = 0.00088$, and so with the choice $T_{*H} = 2500$ K, $E_2/R_u = 11000$ K.

D_2 and n_2 are determined by fitting burning rates. To do this, a homogenized description of the stoichiometric AP/binder blend must be defined, and for this purpose, we use the formulas

$$Q_s = \alpha Q_{s,\mathrm{AP}} + (1-\alpha) Q_{s,B} \tag{34a}$$

$$\rho = \alpha_v \rho_{\mathrm{AP}} + (1-\alpha_v)\rho_B \tag{34b}$$

$$\lambda = \tfrac{1}{2}[\alpha_v \lambda_{\mathrm{AP}} + (1-\alpha_v)\lambda_B] + \tfrac{1}{2}\left[\alpha_v/\lambda_{\mathrm{AP}} + (1-\alpha_v)\big/\lambda_B^{-1}\right] \tag{34c}$$

$$r_b = A \exp\{-E/R_u T_s\} \tag{34d}$$

$$E = \alpha_v E_{\mathrm{AP}} + (1-\alpha_v) E_B \tag{34e}$$

$$A = A_{\mathrm{AP}}^{\alpha_v} A_B^{1-\alpha_v} \tag{34f}$$

where α_v is the volume fraction (packing fraction) of AP. [Formulas (34c), (34e), and (34f) are derived from a homogenization study, which will be described elsewhere.] Thus, $D_2 = 1.2904 \times 10^4$ g · cm^{-3}s^{-1}bar^{-n2}, where $n_2 = 1.75$ (Fig. 4b).

Ex post facto calculations of the one-dimensional structure for the AP/binder blend show that there is some overlap between the two reaction zones so that Eq. (33) is not quite correct, but its use is consistent with the overall accuracy of our model.

The homogenization issue examined here is only one of two that need to be considered in general. Thus, for three-dimensional calculations in particular, the smallest AP particles cannot be resolved numerically and must be accounted for by homogenization.

III. Instabilities in Pure AP Decomposition

Figure 4a is generated by solving the one-dimensional version of the general code in a time-dependent fashion until steady state is achieved. When this is done, oscillating instabilities are uncovered at sufficiently high pressure. These have long been known in the propellant context[15,16] and also in other contexts where they are typically thought of as large-Lewis-number oscillating instabilities. Thus, deflagration studies of an asymptotic nature, valid in the limit of infinite activation energy, identify a stability boundary when the Lewis number is large enough.[17] Because reaction fronts in thermites can be thought of as deflagrations for which $Le = \infty$, it is not surprising that a stability boundary can be found in that context at large enough activation energy.[18,19]

A closely related problem that can display instabilities is the exothermic gasification ($Q_s > 0$) of a solid, without gas-phase combustion, for which the activation energy of the gasification rate r_b is sufficiently large[20]; cordite can behave in this way.[21,22] (A useful survey may be found in Ref. 23.) In other words, our formulation, when restricted to pure AP, is bound to lead to instabilities, even when $R_1 \equiv 0$, if $Q_{s,\mathrm{AP}}$ and E_{AP} are sufficiently large. When they are not, the addition of a gas-phase flame defines a combined reactive structure (surface decomposition plus flame) with a combined Q ($Q_{s,\mathrm{AP}} + Q_{g1}$) and an effective activation energy that can be large enough.

There is a threshold pressure for generating the one-dimensional instability, and in Fig. 5 we show variations in the burning rate with time for various pressures. At 60 atm, the burning is stable; at 80 atm, a periodic instability is apparent; period doubling, a classical path to chaos, is apparent at 110 atm; and yet richer dynamic behavior is apparent at 120 atm.

It is of some interest to examine this instability in a linear context, and to do this, it is first necessary to construct the steady unstable solutions. This also can be done using time integration when use is made of a trick described in Ref. 24: Instead of holding the pressure fixed, as in the standard direct numerical simulation (DNS) calculations, which generate Fig. 5, we fix the integral of R_1 over the gas-phase computational domain. At each fractional time step in the integration (where a Runge–Kutta solver is used), the pressure is adjusted to that end, and convergence to the steady state is achieved. This generates the dashed line of slope 0.8370 in Fig. 6, an extension of the results shown in Fig. 4a. The data points on the dashed line and just below it are mean burning rates defined by the unsteady solution; these show that the one-dimensional instability reduces the mean burning rate. The middle curves of Fig. 6 are discussed later.

Once the steady solution is constructed, the linear equations that describe infinitesimal perturbations from the steady state can be integrated using the same numerical tools as for the nonlinear system. In doing this, we can account for nonplanar disturbances using a modal description in which the disturbances are assumed to contain the factor e^{ikz}, where z is measured parallel to the propellant surface and k is the wave number, an independently assigned parameter.

Figure 7 shows the evolution of perturbations to the burning rate when $k = 0$ for various pressures and shows that the neutral stability for one-dimensional instabilities lies close to a pressure of 59.89 atm.

If there is only a single unstable eigenfunction, the functions drawn in Figs 7b and 7c grow like $e^{\omega t}$ (following initial transients), and ω may be determined from an examination of the function. In this way, the frequency [Im(ω)] and growth rate [Re(ω)] of Fig. 8

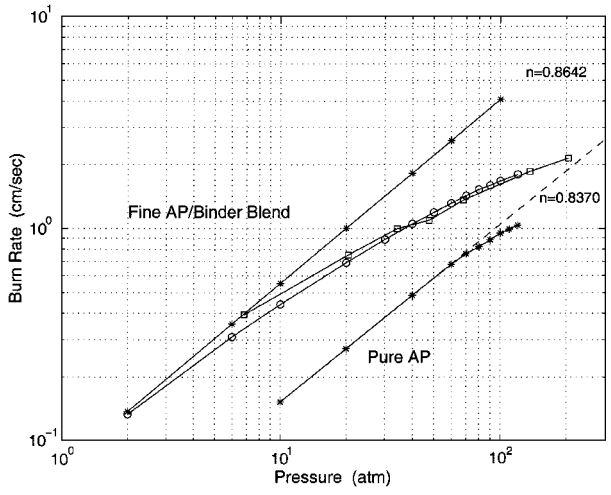

Fig. 6 Mean burning rate vs pressure: upper curve, 1D AP/binder blend (steady) as in Fig. 4a; lower curve, one-dimensional pure AP (steady and unsteady, cf. Fig. 4b, but here the mix is stoichiometric); and middle curves, random disk pack, numerical (○), and experimental data from Ref. 3 (□).

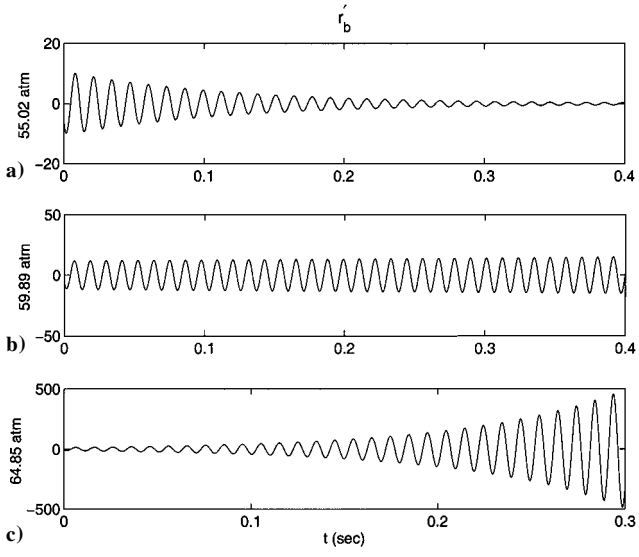

Fig. 7 Variations of the perturbation burning rate of pure AP with time, for different pressures, $k = 0$.

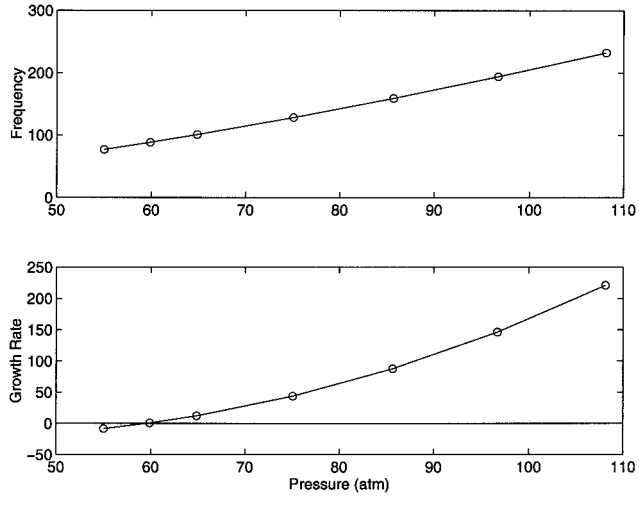

Fig. 8 Frequency and growth rate vs pressure, $k = 0$.

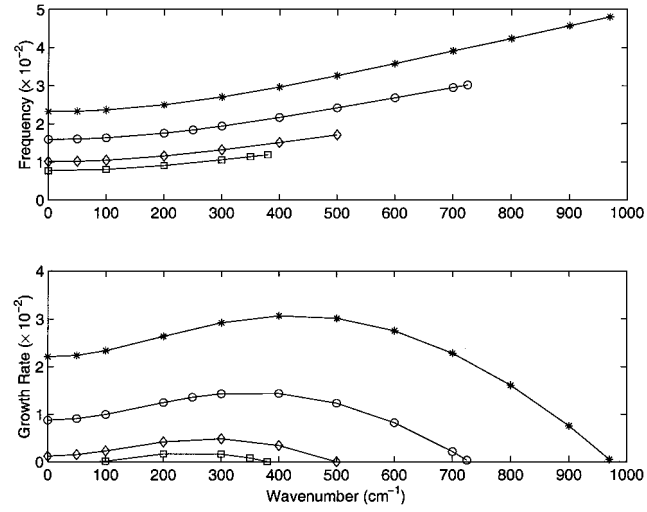

Fig. 9 Variations of frequency and growth rate with wave number for different pressures (from top to bottom): 108.13, 85.68, 64.85, and 55.02.

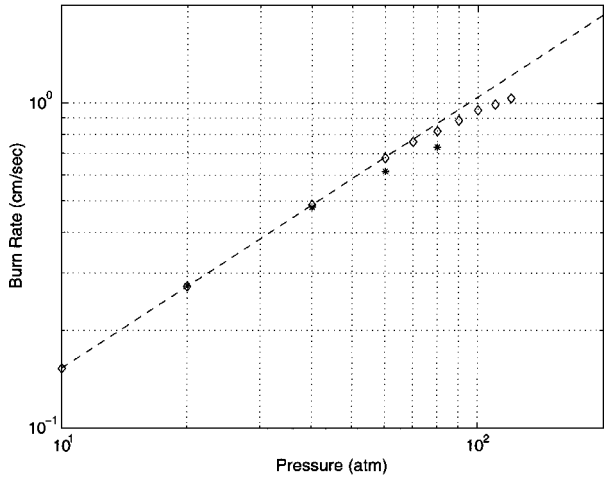

Fig. 10 Mean burning rates for pure AP: ◇, Table 2 data and ∗, $Q_{s,\mathrm{AP}} = 100$ and $Q_{g1} = 230$.

are constructed. The timescales here are, of course, controlled by the condensed phase.

Most of the early discussions of these instabilities in the propellant context are restricted to the one-dimensional case, $k = 0$. An exception is the work of Higuera and Liñán,[16] but their results are expressed within a general nondimensional framework, rather than the AP-specific physical framework that we have adopted here. Figure 9 shows that, when nonvanishing wave numbers are accounted for, there is a modest drop in critical pressure and modest changes in the frequency and growth rate. At 108.13 atm, the most rapidly growing mode is $k \sim 400\ \mathrm{cm}^{-1}$, corresponding to a wavelength of $\sim 157\ \mu$m, which could only fit onto the large AP particles.

What role these instabilities might play in the heterogeneous context is far from clear, nor is it clear how important it is that our model accurately capture the stability details, such as the magnitude of the critical onset pressure. Not surprisingly, partitioning $(Q_{s,\mathrm{AP}} + Q_{g1})$ in different ways affects the results; shifting some of the heat output from the gas phase to the surface lowers the critical pressure. In Fig. 10 we show the mean burning rate both for the data of Table 2 (cf. Fig. 6) and for the choices $Q_{s,\mathrm{AP}} = 100$ and $Q_{g1} = 230$.

One-dimensional DNS calculations for the AP/binder blend revealed no instabilities for the pressures examined here; these simulations exclude both finite wave-number effects, and non-quasi-steady gas-phase effects.

IV. Burning of Random-Pack Propellants and Effects of Particle Size

We define a propellant pack by a periodic array of squares, each randomly packed as in one of the packs shown in Fig. 3. To describe the burn through of a single square, one or more squares are first consumed to ensure that periodic burning has been achieved, that is, that the consumption of the square is independent of the initial conditions.

Although each of the packs of Fig. 3 uses the same particles (Table 1), the different arrangements have an effect on the burn-through time, but one that does not exceed 2%. Similar variations are generated if a pack is rotated through 90, 180, or 270 deg. These variations would be even smaller for large packs, that is, packs using more particles.

Note that there are nominally 100 particles in each pack, with diameter nominally 100 μm, so that 10 of them intersect a side (1000 μm long) and the total disk area $\sim\pi/4\times10^{-2}\text{cm}^2$, corresponding to a packing fraction $\sim\pi/4$. For a regression speed $c=0.69$ cm/s, the thermal wave thickness in the AP, defined by $\lambda_{\text{AP}}/\rho_{\text{AP}}cc_p$ is approximatley 24 μm, and the thermal wave thickness in the binder $\lambda_B/\rho_B cc_p$ is approximately 34 μm. In the gas, at a temperature of 1000 K, and with a mass flux M of 1.202 g/cm^{2}s, λ_g/Mc_p is approximately 8 μm. The burn-through time of a square is approximately 0.1445 s and for a single particle $\sim$0.015 s.

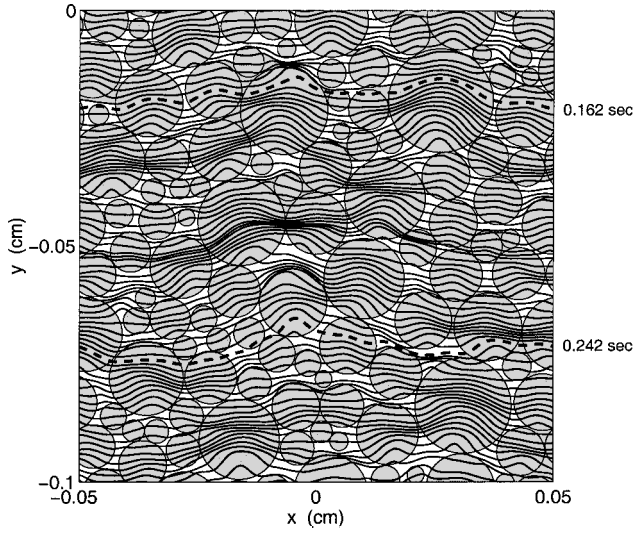

Fig. 11 Surface location at time intervals of 0.002 s over the time interval ~ 0.136− 0.261 s for pack 1, at 20 atm.

Figure 11 shows the burn through of pack 1 at a pressure of 20 atm. (These results, like all those that we show, were generated using the Oseen model. Spot checks using the full Navier–Stokes code revealed negligible differences for all quantities except, of course, the x component of velocity.) The lines represent the surface location at time intervals of 0.002 s in a burn-through interval $\sim$0.136 − 0.280 s. When a significant portion of the surface consists exclusively of AP, the local regression is slow compared to that of portions where significant mixing of AP and binder can occur. For example, the surface curves crowd together near $x=0.0$ cm, $y=-0.05$ cm, but are spread out near $x=-0.05$ cm, $y=-0.05$ cm.

The nature of the combustion field is shown by Fig. 12, which gives an indication of $Q_t=Q_{g1}R_1+Q_{g2}R_2$, also at a pressure of 20 atm. The two times, 0.162 and 0.242 s, are marked in Fig. 11. The horizontal flame structures are AP decomposition flames; the vertical structures are diffusion flames. Note that the base of each diffusion flame lies, not at the AP/binder interface, but on the AP. This noticeable displacement is a consequence of the stoichiometry and the flux conditions (23) and has been discussed in simpler contexts.[25]

For $t=0.242$ s, there is a portion of the surface, a cut through a region of fuel binder, that is shorn of flame structures. This can be seen at the 11 o'clock position relative to the large AP particle in the lower right-hand corner. Should there be a large number of such regions, so that the flame-structures are heavily fractured, it may be anticipated that extinction would occur, a percolation theory phenomenon. This would happen if the pack were excessively fuel rich.

Fluctuations in a number of surface-defined quantities are shown in Figure 13.

1) Surface area deviations are modest because the surface remains fairly flat.

2) The mass flux is the instantaneous surface integral of the flux through the surface; the average value is 1.202 g/cm^{2}s.

3) The equivalence ratio is flux based; it is the ratio of the instantaneous mass flux of binder to that of AP, normalized with the

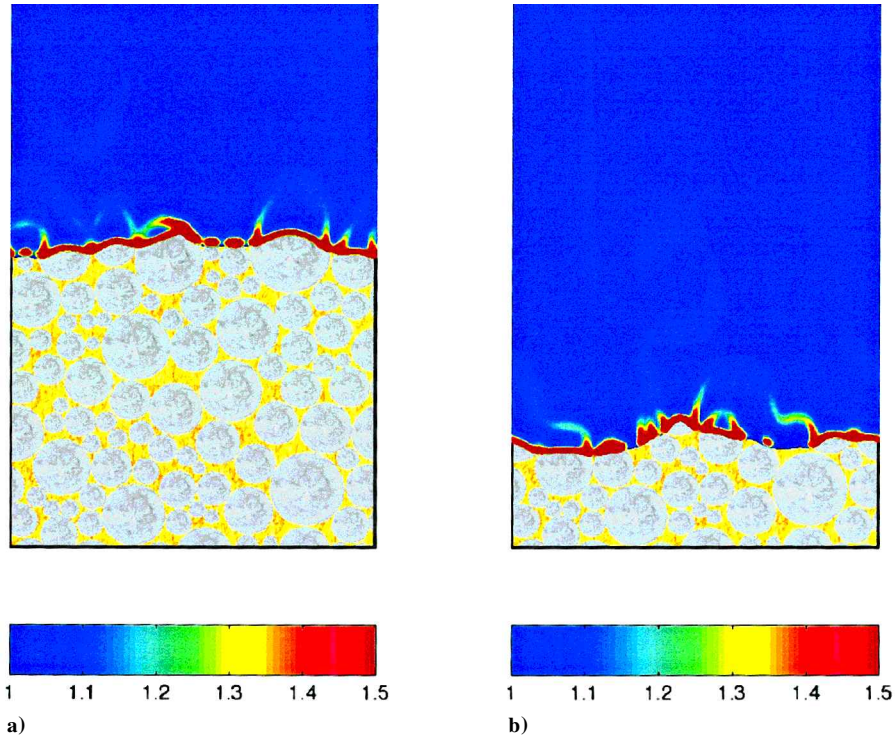

Fig. 12 Combustion field for pack 1, 20 atm: color shading indicates the values of $1+10^{-6}(Q_{g1}R_1+Q_{g2}R_2)/c_p$, which has a maximum of a) 8.2632 g · K/cm^{3}s for $t=0.162$ s and b) 7.2811 g · K/cm^{3}s for $t=0.242$ s. All values greater than 1.5 are assigned a single color.

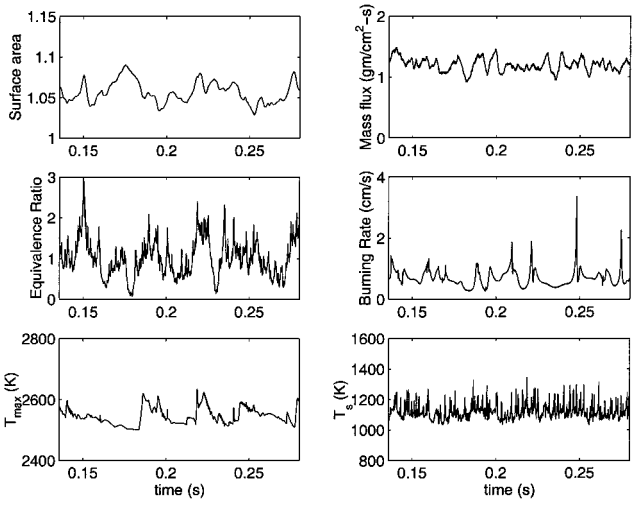

Fig. 13 Fluctuations in various surface variables with time for pack 1, at 20 atm.

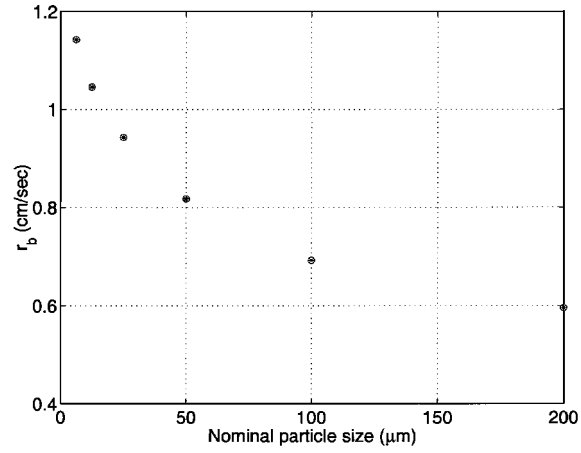

Fig. 14 Variations in burning rate with nominal AP size, at 20 atm.

stoichiometric ratio of these fluxes. During a burn through, there are intervals for which the flux is significantly fuel lean, and others where it is significantly fuel rich.

4) The burning rate is defined as the regression speed at the boundaries $x = \pm 0.05$ cm and can be compared with the surface spacing of Fig. 12. The mean value is approximately 0.69 cm/s, and the excursions from this are significant.

5) $T_{\max}$ is the instantaneous maximum temperature in the combustion field. There are modest variations about the adiabatic flame temperature 2500 K.

6) T_s is the instantaneous maximum surface temperature.

These fluctuations raise an important question: What is the effect on the turbulent flow within the chamber? In Ref. 26, recent cold-flow experiments are described in which air is drawn through the porous side walls of a channel. Different pore sizes lead to different mean core flows, ranging from the classical Culick solution[27] (also see Ref. 28) to one that looks similar to a classical turbulent channel flow. The implications are that the small-scale nature of the flow-field near the surface can strongly affect the nature of the core flow but in ways that we do not understand at the present time.

Figure 6 (burn rate vs pressure) shows two sets of data that we have not yet discussed, marked by circles and squares. The circles are numerical results for pack 1, delimited by the pure AP and AP/binder blend results. At the present time, due to the lack of an adaptive mesh refinement tool, we are unable to carry out calculations above ~120 atm, and so the interesting question of what happens at high pressures remains to be addressed.

The squares in Fig. 6 are experimental burning rates for the Miller pack[3] SD-III-88-24 (see Fig. 1) and are in unexpected agreement with the numerical results; the experimental configuration is, of course, three dimensional, and the pack contains a large amount of fine powder to achieve stoichiometry. Thus, the agreement is fortuitous, but we show it to indicate that the model can capture experimental trends. In due course we expect to carry out three-dimensional calculations for a pack that represents the Miller pack, and these comparisons will have greater significance.

The results that we have presented so far are for packs defined by Table 1. Each pack is a square of side 1000 μm (cf. Fig. 11) and contains 101 particles, defining a nominal particle size of 100 μm (~10 particles per side). The same packing data can be modified to construct packs of particles of different nominal size. To do this, we pack $n(101)$ particles (where n is an integer) into a rectangle of height 1000 μm and a width that (along with n) controls the nominal particle size. The size distribution is fixed: If $n = 4$, there are 4 largest particles and 20 smallest particles, and the ratio of their diameters is $220.744/35.784 = 6.169$, but the actual diameters are only 220.744 and 35.784 μm for a pack width of 4000 μm. Thus, if $n = 2$ (202 particles) and the width is 500 μm, the particle diameters are halved, and the nominal diameter is 50 μm (~20 particles per 1000 μm side and ~10 particles per 500 μm side).

Figure 14 shows variations in the burning rate with the nominal particle diameter for a pressure of 20 atmospheres, and reproduces the well-known fact that the smaller are the particles in the pack the more rapid is the regression rate. Some insight into this phenomenon is described in Ref. 6, reproduced in slightly different form here.

Consider the generic reaction–diffusion problem

$$M\frac{\partial \phi}{\partial y} = \rho \mathrm{D}\left(\frac{\partial^2 \phi}{\partial x^2} + \frac{\partial^2 \phi}{\partial y^2}\right) + \Omega, \qquad y > 0, \qquad |x| < L \quad (35)$$

Halving L is equivalent to keeping L fixed and making the substitution $x \to \frac{1}{2}x$, whence the equation for ϕ becomes

$$M\frac{\partial \phi}{\partial y} = \rho \mathrm{D}\left(4\frac{\partial^2 \phi}{\partial x^2} + \frac{\partial^2 \phi}{\partial y^2}\right) + \Omega \quad (36)$$

Thus, reducing L is equivalent to introducing anisotropic diffusion, augmenting the x-wise diffusion but not the y-wise diffusion. This speeds up mixing between the components of the R_2 reaction.

V. Conclusions

For many decades, the theoretical framework within which heterogeneous propellant burning has been discussed has consisted of a two-dimensional physical picture forced into a one-dimensional mathematical model.[4] This has obviously been of value, and important insights have been achieved, but we believe that it is time to adopt a new paradigm: a multidimensional numerical framework of the kind that we have described here. The key to our approach is a strategy for representing the propellant morphology as randomly packed spheres of AP.[1,2] With this in place, a fully coupled description of the gas phase, condensed phase, and moving surface allows for an examination of fundamental questions of propellant burning.

The specific model that we have used here is a simple one, indeed oversimplified, and one that omits much physics; in a word, it is false. However, unless we have made numerical errors, our results are not wrong. Indeed, right and wrong is not the correct dichotomy within which to evaluate the results. What is important is the extent to which they imitate the burning of real propellants, and there are things to be learnt from both its failures and its successes in this respect. We anticipate an evolutionary process in which new ingredients will be added and existing ingredients modified, and we are confident that there will be useful successes despite that for such a complex problem the model will be eternally false.

There are a number of issues that we have discussed, although much is unresolved. Exothermic multiphase processes are susceptible to intrinsic oscillating instabilities, there is a large literature on the subject, and our model for AP decomposition exhibits such instabilities at high enough pressures. These would undoubtedly be affected by melt layers, in-depth condensed-phase reaction, more complex gas-phase kinetics, etc., but how important they are in the description of heterogeneous propellant burning is not clear. We demonstrate a modest impact on the mean burning rate of pure AP for pressures ~100 atm.

The speed with which the surface of a randomly packed propellant recedes depends on the local distribution of AP and binder. An excess of binder can lead to extinction, an excess of AP leads to modest regression driven by the AP deflagration, and a mix of AP and binder leads to rapid regression augmented by the heat of the AP/binder reaction. All of these effects are apparent from Figs. 11 and 12. There are a number of related issues to be explored: the effects of AP size, the effects of AP size distribution (e.g., the large/small AP size ratio for a bimodal propellant), the effects of stoichiometry (e.g., extinction for fuel-rich propellants), extinction pressure intervals, etc. Of particular interest would be three-dimension calculations for the various Miller packs[3] for which mean burning-rate predictions could be compared with the experimental data. These require a parallelized code running on ASCI-level machines.

Large fluctuations in surface-integrated quantities (mass flux, equivalence ratio) occur during a burn through. Our calculations are for a square of propellant of side $L = 1000\ \mu$m, and clearly the magnitude of the fluctuations would be different for different values of L, vanishing as $L \to \infty$. An examination of these variations with L can define a length scale, characteristic of the fluctuations, of the kind fixed in the cold-flow rocket simulation experiments of Ref. 26 by the choice of pore size in the porous walls. How these fluctuations affect the core flow is a difficult unsolved problem but one that must eventually be addressed. The reverse problem, how the core flow affects the burning rate (erosive burning), is an equally difficult problem, one that cannot be seriously addressed without a propellant burning model of the kind we have described here.

Acknowledgments

This work was supported by the U.S. Department of Energy through the University of California under Subcontract B341494. J. Buckmaster is also supported by the Air Force Office of Scientific Research and by NASA John H. Glenn Research Center at Lewis Field. The packs used in the calculations were generated by S. Kochevets.

References

[1]Knott, G. M., Jackson, T. L., and Buckmaster, J., "The Random Packing of Heterogeneous Propellants," *AIAA Journal*, Vol. 39, No. 4, 2001, pp. 678–686.

[2]Kochevets, S., Buckmaster, J., Jackson, T. L., and Hegab, A., "Random Packs and Their Use in the Modeling of Heterogeneous Solid Propellant Combustion," *Journal of Propulsion and Power*, Vol. 17, No. 4, 2001, pp. 883–891.

[3]Miller, R. R., "Effects of Particle Size on Reduced Smoke Propellant Ballistics," AIAA Paper 82-1096, 1982.

[4]Beckstead, M. W., Derr, R. L., and Price, C. F., "Model of Composite Solid-Propellant Combustion Based on Multiple Flames," *AIAA Journal*, Vol. 8, No. 12, 1970, pp. 2200–2207.

[5]Cai, W., and Yang, V., "Model of AP/HTBP Composite Propellant Combustion," AIAA Paper 2000-0311, 2000.

[6]Hegab, A., Jackson, T. L., Buckmaster, J., and Stewart, D. S., "Nonsteady Burning of Periodic Sandwich Propellants with Complete Coupling Between the Solid and Gas Phases," *Combustion and Flame*, Vol. 125, No. 2, 2001, pp. 1055–1070.

[7]Price, E. W., Handley, J. C., Panyam, R. R., Sigman, R. K., and Ghosh, A., "Combustion of Ammonium Perchlorate–Polymer Sandwiches," *AIAA Journal*, Vol. 19, No. 3, 1981, pp. 380–386.

[8]Price, E. W., "Effects of Multidimensional Flamelets in Composite Propellant Combustion," *Journal of Propulsion and Power*, Vol. 11, No. 4, 1995, pp. 717–728.

[9]Smooke, M. D., Yetter, R. A., Parr, T. P., and Hanson-Parr, D. M., "Experimental and Modeling Studies of Two-Dimensional Ammonium Perchlorate Flames," *Proceedings of the Combustion Institute*, Vol. 28, No. 1, 2000, pp. 839–846.

[10]Rasmussen, B., and Frederick, R. A., Jr., "A Nonlinear Heterogeneous Model of Composite Solid Propellant Combustion," AIAA Paper 99-2228, 1999.

[11]Sutton, G. P., *Rocket Propulsion Elements*, 6th ed., Wiley-Interscience, New York, 1992, p. 450.

[12]Cohen, N. S., and Strand, L. D., "Improved Model for the Combustion of Ammonium Perchlorate Composite Propellants," *AIAA Journal*, Vol. 20, No. 12, 1982, pp. 1739–1746.

[13]Jeppson, M. B., Beckstead, M. W., and Jing, Q., "A Kinetic Model for the Premixed Combustion of a Fine AP/HTPB Composite Propellant," *34th JANNAF Combustion Meeting*, CPIA Publication 662, Chemical Propulsion Information Agency, Laurel, MD, 1997, pp. 117–129.

[14]Beckstead, M. W., Tanaka, M., Jing, Q., and Jeppson, M. B., "An Ammonium Perchlorate Model Based on a Detailed Mechanism," *33rd JANNAF Combustion Meeting*, CPIA Publication 638, Chemical Propulsion Information Agency, Laurel, MD, 1996, pp. 41–46.

[15]Zanotti, C., Carretta, U., Grimaldi, C., and Colombo., G., "Self-Sustained Oscillatory Burning of Solid Propellants: Experimental Results," *Nonsteady Burning and Combustion Stability of Solid Propellants*, edited by L. De Luca, E. W. Price, and M. Summerfield, Vol. 143, Progress in Astronautics and Aeronautics, AIAA, Washington, DC, 1992, pp. 399–439.

[16]Higuera, F. J., and Liñán, A., "Stability of solid propellant combustion subject to nonplanar perturbations," *Dynamics of Flames and Reactive Systems*, edited by J. R. Bowen, N. Manson, A. K. Oppenheim, and R. I. Soloukhin, Vol. 95, Progress in Astronautics and Aeronautics, AIAA, New York, 1984, pp. 248–258.

[17]Sivashinsky, G. I., "Diffusional–Thermal Theory of Cellular Flames," *Combustion Science and Technology*, Vol. 15, No. 1, 1977, p. 137.

[18]Makhviladze, G. M., and Novozhilov, B. V., "Dvumernaya Ustoichivost Goreniya Kondensirovannykh Sistem (The Two-Dimensional Stability of Combustion in Condensed Systems)," *PrikladnayaMekh.Tekh.Fiz.*, Vol. 3, No. 4, 1962, p. 21.

[19]Maksimov, E. I., and Shkadinski, K. G., "Ob Ustoichivosit Statsionarnogo Goreniya Bezgazovykh Sostavov (On the Stability of Stationary Combustion in Gasless Compositions)," *Fiziki Goreniya Vzrva*, Vol. 7, No. 3, 1971, p. 454.

[20]Zeldovich, Y. B., "K Teorii Goreniya Porokhov i Vzryvchcitykh Veschestv (On the Theory of Combustion of Powders and Explosives)," *Zhurnal Eksperimental' noi i Teoreticheskoi Fiziki (Soviet Physics—JETP)*, Vol. 12, No. 11/12, 1942, pp. 498–524.

[21]Huffington, J. D., "The Burning and Structure of Cordite," *Transactions of the Faraday Society*, Vol. 47, No. 3, 1951, pp. 864–876.

[22]Huffington, J. D., "The Unsteady Burning of Cordite," *Transactions of the Faraday Society*, Vol. 50, No. 3, 1954, pp. 942–952.

[23]Williams, F. A., *Combustion Theory*, 2nd ed., Benjamin/Cummings, Menlo Park, CA, 1985, p. 328.

[24]Buckmaster, J., "Large-Lewis-Number Instabilities of Edge-Flames," *Combustion and Flame*, Vol. 127, No. 4, 2001, pp. 2223–2233.

[25]Buckmaster, J., Jackson, T. L., and Yao, J., "An Elementary Discussion of Propellant Flame Geometry," *Combustion and Flame*, Vol. 117, No. 3, 1999, pp. 541–552.

[26]Deng, Z., Adrian, R. J., and Tomkins, C. D., "Structure of Turbulence in Channel Flow with a Fully Transpired Wall," AIAA Paper 2001-1019, 2001.

[27]Culick, F. E. C., "Rotational Axisymmetric Mean Flow and Damping of Acoustic Waves in Solid Propellant Rocket Motors," *AIAA Journal*, Vol. 4, No. 8, 1966, pp. 1462–1464.

[28]Proudman, I., "An Example of Steady Laminar Flow at Large Reynolds Number," *Journal of Fluid Mechanics*, Vol. 9, 1961, pp. 593–602.

J. R. Bellan
Associate Editor